Original Article
Metabolic characteristics distinguishing intrahepatic cholangiocarcinoma: a negative pilot study of 18F-fluorocholine PET/CT clarified by transcriptomic analysis

Sandi A Kwee[1,2], Gordon S Okimoto[1], Owen TM Chan[1], Maarit Tiirikainen[1], Linda L Wong[1]

[1]Cancer Biology Program, The University of Hawaii Cancer Center, Honolulu, Hawaii, USA; [2]Hamamatsu/Queen's PET Imaging Center, The Queen's Medical Center, Honolulu, Hawaii, USA

Abstract: PET using fluorine-18 fluorocholine (18F-fluorocholine) may detect malignancies that involve altered choline metabolism. While 18F-fluorocholine PET/CT has shown greater sensitivity for detecting hepatocellular carcinoma (HCC) than 18F-fluoro-D-deoxyglucose (FDG) PET/CT, it is not known whether it can also detect intrahepatic cholangiocarcinoma (ICC), a less common form of primary liver cancer. Clinical, radiographic, and histopathologic data from 5 patients with ICC and 23 patients with HCC from a diagnostic trial of liver 18F-fluorocholine PET/CT imaging were analyzed to preliminarily evaluate 18F-fluorocholine PET/CT for ICC. Imaging was correlated with whole-genome expression profiling to identify molecular pathways associated with tumor phenotypes. On PET/CT, all ICC tumors demonstrated low 18F-fluorocholine uptake with a significantly lower tumor to mean background uptake ratio than HCC tumors (0.69 vs. 1.64, p < 0.0001), but no corresponding significant difference in liver parenchyma uptake of 18F-fluorocholine between ICC and HCC patients (8.0 vs. 7.7, p = 0.74). Two ICC patients demonstrated increased tumor metabolism on FDG PET/CT, while immunohistochemical analysis of ICC tumors revealed overexpression of glucose transporter 1 (GLUT-1) and hexokinase indicating a hyper-glycolytic phenotype. Gene expression analysis revealed down-regulation of farnesoid-X-receptor and other lipid pathways in ICC relative to HCC, and up-regulation of glycolytic pathways and GLUT-1 by HIF1α. These results imply limited utility of 18F-fluorocholine in ICC, however, significant metabolic differences between ICC, HCC, and parenchymal liver tissue may still provide clues about the underlying liver pathology. Gene and protein expression analysis support hyperglycolysis as a more dominant metabolic trait of ICC.

Keywords: Cholangiocarcinoma, hepatocellular carcinoma, positron emission tomography, fluorocholine

Background

Cholangiocarcinoma is a malignancy that originates from biliary epithelia and arises either as an extra-hepatic lesion in the biliary tree, or less commonly, as a mass lesion within the liver parenchyma itself. The latter, termed intrahepatic cholangiocarcinoma (ICC), historically has accounted for only 10% of all primary liver cancers, however its incidence appears to be increasing in some regions [1]. It is difficult to explain the increasing incidence based on established risk factors for cholangiocarcinoma. Risk factors for cholangiocarcinoma typically associate with chronic biliary inflammation, and include primary sclerosing cholangi-tis, liver parasitic infection, and congenital abnormalities of the biliary tract. More recent studies have identified viral hepatitis, cirrhosis, diabetes, obesity, and alcohol consumption as potential additional ICC risk factors [2]. These are also risk factors for hepatocellular carcinoma (HCC), the most common primary liver cancer and one that is also rising in incidence. Due to the increasing incidence of HCC and ICC, it is becoming more important to confidently discriminate between these liver tumors, particularly since ICC is refractory to several treatments for HCC [3-5].

Extra-hepatic cholangiocarcinoma, which is more common than ICC, frequently presents

with signs of biliary obstruction before forming a significant mass. Thus it is rarely confused with HCC. In contrast, ICC is mass-forming and there is a growing appreciation that its radiographic appearance can vary substantially and overlap with HCC [3]. Histology obtained from percutaneous biopsies also may not consistently differentiate ICC from HCC variants and metastatic adenocarcinoma, and while clinical risk factors, cirrhosis severity, and serum tumor markers such as cancer antigen 19-9 (CA 19-9) may be helpful, the diagnosis of liver tumors may ultimately rely on tissue examination after hepatic resection [2, 3].

An investigational positron emission tomography (PET) technique for imaging choline metabolism using the radiopharmaceutical tracer fluorine-18 fluorocholine (^{18}F-fluorocholine) has recently shown clinical utility for detecting HCC [6]. However, there is little data on imaging other liver tumors with ^{18}F-fluorocholine. There is also limited data on the molecular changes that may lead to specific radiographic and molecular imaging phenotypes in liver cancer. This pilot study is the first to report findings on ^{18}F-fluorocholine PET/CT in ICC, and does so in conjunction with gene and protein expression analysis in an attempt to further inform the development of molecular imaging strategies for liver tumors.

Methods

Patients

Among patients taking part in a U.S. registered clinical trial of liver PET/CT imaging using ^{18}F-fluorocholine PET/CT (NIH NCT01395030), 5 patients were identified as diagnosed with ICC based on post-surgical histopathology. In addition to reviewing tumor radiologic and histopathologic features from these 5 patients, a transcriptomic analysis was conducted to compare whole-genome gene expression profiles available from 3 of the ICC tumors and 23 HCC tumors collected consecutively from other patients participating in the trial.

Written informed consent was obtained from all patients in accordance with an institutional review board approved clinical research protocol that adheres to the ethical guidelines of the Declaration of Helsinki and its subsequent amendments. All patients were recruited to the

study by hepatobiliary/transplant surgeons affiliated with a single-institution multi-disciplinary liver disease management program. Clinical records were used to collect data on patient demographics and liver disease risk factors such as infection by viral hepatitis and significant alcohol use (defined as at least 2 alcoholic beverages daily for 10 years). The study also collected clinical laboratory data, including bilirubin, alkaline phosphatase, albumin, and tumor markers including CA 19-9 and alpha-fetoprotein levels.

Tumor and non-tumor liver tissue samples were collected for research at the time of hepatic resection if agreed upon by the attending surgeon. Collected samples were divided using sterile instruments and placed into formalin, liquid nitrogen, and RNA-preservative (RNALater, Thermo Fisher Scientific, Waltham, Massachusetts). These samples were stored under appropriate conditions until further analysis.

Fluorine-18 fluorocholine synthesis

Fluorine-18 fluorocholine synthesis was performed by fluorination of ditosylmethane with fluorine-18 followed by alkylation of the fluorotosylmethane intermediate with dimethylethanolamine using a chemical process control unit (CTI/Siemens CPCU, CTI/Siemens, Knoxville, TN) [7]. All synthesis products passed standard assays for radiochemical purity, radionuclide identity, chemical purity, and non-pyrogenicity prior to injection. Radiochemical purity was greater than 99%.

PET/CT imaging

PET/CT imaging was performed with a Philips Gemini TF-64 PET/CT scanner (Philips Healthcare, Andover, Massachusetts) using ^{18}F-fluorocholine under an investigational new drug protocol. A CT scan without intravenous contrast was first performed in the supine position. The 64-channel helical CT scanning parameters were: 120 kV, 50 mA/slice, rotation time 0.75 seconds, slice thickness/interval 5.0 mm. Following injection of 2.2 to 3.0 MBq/kg of the tracer through a peripheral intravenous line, dynamic emission scanning was conducted for the first 40 minutes of radiopharmaceutical distribution, after which static PET scans of the liver were obtained. PET image reconstruction was performed using a maximum likelihood

Table 1. Patient demographic, imaging, and immunohistochemical findings

ID	Age	Gender	Size (cm)	SUV Ratio	GLUT-1		HK		CKA		HIF1	
					tu	nl	tu	nl	tu	nl	tu	nl
1	52	F	5.5	0.65	2	1	2	2p	2	2	2	1
2	63	M	4.2	0.66	2	0	2	1	2	2	1	0
3	65	M	3.5	0.87	2c	0	0	2	2	1	2c	0
4	54	M	7.4	0.75	2	0	2	2p	2	2	2	2p
5	56	M	6.5	0.51	2	1	2	1p	2	1	2	1p

IHC stain intensity was rated as: 0 = absent or weak, 1 = modest, 2 = moderate, and 3 = intense. GLUT-1 intensity was rated for the cell membrane and HIF-1 expression was rated for the nucleus. Abbreviations are as follows: SUV = standardized uptake ratio, GLUT-1 = glucose transporter-1, HK = hexokinase, CKA = choline kinase alpha, HIF1 = hypoxia inducible factor 1, tu = tumor tissue, nl = native liver tissue, p = patchy cellular distribution, c = cytoplasmic localization only.

Table 2. Laboratory values of patients diagnosed with ICC

Patient	Bili-rubin	Alk Phos	AFP	Ca 19-9	HBsAg	HBcAg	HCV
1	0.4	80	3	1	No	No	No
2	9.6	167	12	2,871	No	No	No
3	0.5	84	2.9	34	Yes	No	No
4	0.4	186	133	376	No	No	No
5	0.2	128	2.6	108	No	No	No

AFP = alpha fetoprotein, CEA = carcinoembryonic antigen, CA 19-9 = cancer antigen 19-9, HBsAg = hepatitis B surface Antigen, HBcore = hepatitis B core antigen, HCV = hepatitis C virus.

expectation maximization algorithm using CT data for attenuation correction.

PET/CT images were reviewed on a multi-modality imaging workstation (Hybrid PDR, version 1.4c; Hermes Medical Solutions). Liver lesions were identified on PET/CT in correlation with available clinical radiographic examinations and a volume region of interest (ROI) was placed around the tumor region. The standardized uptake value (SUV), defined as the measured radioactivity of a pixel divided by the injected radioactivity normalized to body weight, was used as the measure of tissue uptake on static PET images and the maximum SUV (SUVmax) of each ROI was determined. A tumor to mean background ratio (TBR) was calculated for all liver tumors by dividing the tumor SUVmax by the average SUV corresponding to a 2 cm diameter ROI placed in the liver parenchyma adjacent to the tumor ROI.

Gene expression array analysis

In 3 cases of moderately-differentiated ICC, there was tissue sample material of sufficient quality for transcriptional analysis. Gene expression profiles from these samples were compared to the tumor expression profiles from 23 consecutive HCC patients that had also underwent 18F-fluorocholine PET/CT before surgery. First, RNA was extracted from homogenized frozen tissue lysates in RLT Plus buffer with the AllPrep DNA/RNA Mini kit (Qiagen, Valencia, CA) following manufacturer's protocol. The isolated RNA was stored at -80°C until used. The quality of the total RNAs was checked on a Bioanalyzer using RNA 6000 Nano chips (Agilent, Santa Clara, CA). The isolated RNA was processed following the Illumina whole-genome cDNA-mediated annealing, selection, extension, and ligation protocol with resulting polymerase chain reaction products hybridized onto the Illumina HumanHT-12 v4 Expression BeadChips (Illumina Inc., Sunnyvale, California). Arrays were scanned using the iScan™ instrument and expression levels were quantified using GenomeStudio software (Illumina Inc., Sunnyvale, CA).

Gene expression array data consisted of the expression levels of 20792 genes for 26 patients. The array data was pre-processed by generalized log2 transformation with background subtraction, quantile normalization, and row centering [8]. Sparse rank-1 matrix factorizations were used to identify a small number of genes that characterized global differences in gene expression between the ICC and HCC samples with false discovery rate (FDR) estimated by permutation testing.

An analysis for activated gene pathways, upstream regulators, downstream targets, and biological effects was performed using Ingenuity Pathway Analysis software (IPA, QIAGEN Redwood City, California). This software served to identify molecular mechanisms that may be responsible for the observed differences in gene expression between the ICC and HCC
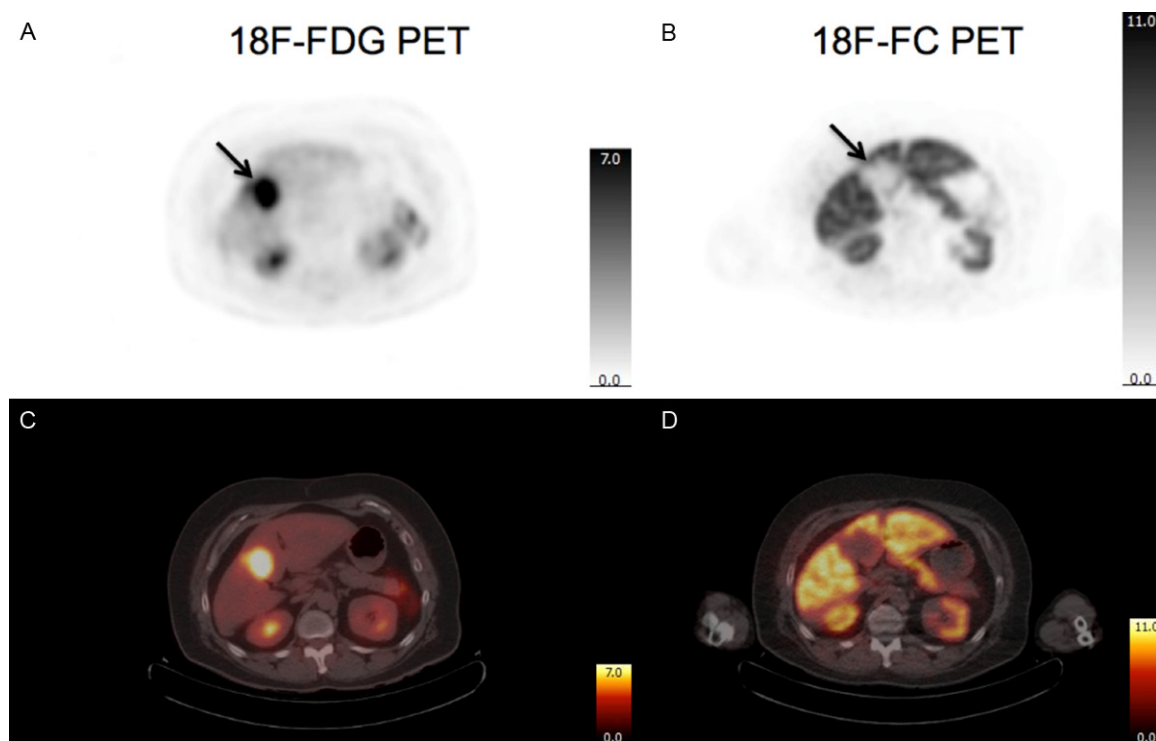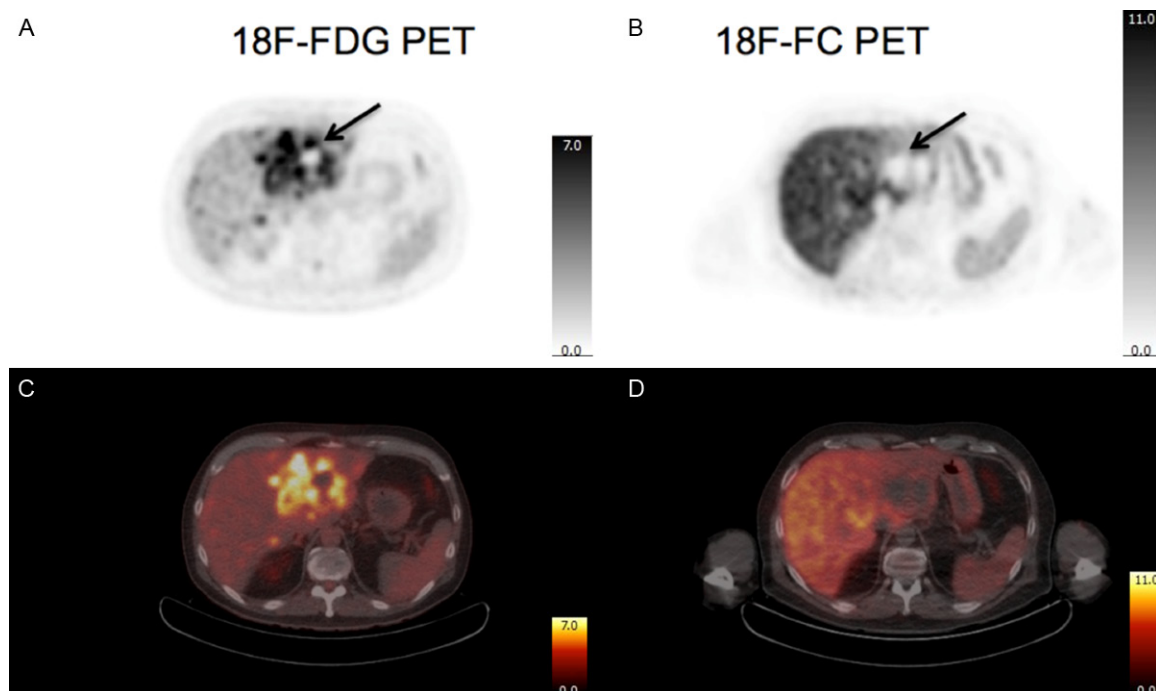
Figure 1. Intrahepatic cholangiocarcinoma demonstrating low ^{18}F-fluorocholine uptake and uniformly high ^{18}F-FDG uptake. Image intensity scale is in SUV units. A liver mass was incidentally detected on ^{18}F-FDG PET/CT in Patient 1 during clinical radiographic follow-up of breast cancer. FDG PET (A) and PET/CT (C) images demonstrate increased FDG uptake corresponding to a 4.0 cm mass in the right hepatic lobe (arrow). In contrast, PET (B) and corresponding PET/CT (D) images obtained following administration of ^{18}F-fluorocholine show diminished radiopharmaceutical uptake by the tumor. Surgical pathology confirmed the diagnosis of moderately differentiated ICC.

samples. Candidate upstream regulators of a given signature were ranked by the degree to which the change in expression of their downstream targets was consistent with the current biomedical literature (Score) and the likelihood that the observed intersection of target genes with the signature was a chance event (*P*-value). Upstream regulators with scores greater than 2.0 and *P*-values less than 0.01 were considered significant. The downstream targets of top-ranked upstream regulators were then further analyzed in IPA to identify genes and pathways associated with specific disease functions and biological processes such as cellular growth and proliferation, inflammatory response, angiogenesis, and lipid metabolism.

Validation by immunohistochemistry

Tumor and liver tissue were taken from the surgical resection specimen, fixed with 10% formalin, and embedded in a paraffin block. Immunohistochemical (IHC) analysis of de-paraffinized rehydrated tumor and parenchymal tissues was performed using an automated

antibody staining platform (Dako, Inc., Carpinteria, CA, USA). Choline kinase alpha (CKA) was evaluated using a commercial antibody (choline kinase alpha rabbit polyclonal antibody, Sigma-Aldrich Co. LLC., St. Louis, Missouri) in accordance with the manufacturer's protocol and an antibody dilution to 1:30. Hexokinase-2 (HK2) was evaluated using a commercial antibody (hexokinase II rabbit monoclonal antibody, Cell Signaling Technology, Inc., Danvers, Massachusetts) with antibody dilution adjusted to 1:100. Glucose transporter-1 (GLUT-1) expression was evaluated using a commercial antibody (Glucose Transporter 1 rabbit monoclonal, Cell Marque, Rocklin, California) with antibody dilution adjusted to 1:100. Hypoxia inducible factor 1 alpha (HIF1A) expression was evaluated using a commercial antibody (Hα111a mouse monoclonal, Enzo, Life Sciences, Inc., Farmingdale, New York) with antibody dilution adjusted to 1:100. Antibody detection was conducted using a horseradish peroxidase HiDef polymer detection system with diaminobenzidine as substrate (Cell Marque, Rocklin, California). A hepatobiliary pathol-

Figure 2. Intrahepatic cholangiocarcinoma demonstrating heterogeneously increased ^{18}F-FDG uptake but low ^{18}F-fluorocholine uptake. Image intensity scale is in SUV units. Patient 4 presented with a liver mass detected on ultrasound. FDG PET (A) and PET/CT (C) images demonstrate an area of heterogeneously increased FDG uptake corresponding to a 7.4 cm mass in the left hepatic lobe (arrow). Corresponding ^{18}F-fluorocholine PET (B) and PET/CT (D) images show diminished ^{18}F-fluorocholine uptake in this region. The diagnosis of moderately differentiated ICC was established by surgical pathology examination of the tumor.

ogist (OC) visually evaluated each section at 200X and 400X, grading each tumor and liver tissue specimen based on a standardized scoring system adapted for evaluating liver tumors, with marker intensity rated on an ordinal scale from 0 (no staining) to 3 (intense staining), cell distribution classified as patchy or diffuse, and the predominant cellular localization (nucleus, cytoplasm, or membrane) identified for each antibody [9, 10].

Statistical analysis

Descriptive and general statistical calculations were performed using JMP 11 Pro (SAS Institute, Inc., Cary, NC). Categorical comparisons (i.e. ICC patients vs. HCC patients) were conducted by t-test. All tests were two-tailed and a *p*-value < 0.05 was considered statistically significant unless otherwise stated.

Results

Each patient underwent a partial hepatectomy with histopathologic examination of the primary tumor confirming the final cancer diagnosis. Tumor diameter ranged from 1.2 cm to 6.5 cm

measured in the longest axis on gross pathology examination prior to formalin fixation. ICC tumors were classified by histology as moderately differentiated in 4/5 patients and well differentiated in one patient (Patient 3).

Patient clinical parameters are summarized in **Table 1**. None of the 5 patients with ICC had a clinical history of underlying cirrhosis or classical risk factors for ICC, although one patient had chronic HBV infection. Laboratory values and hepatitis serology are summarized in **Table 2**.

PET imaging findings

Tumor ^{18}F-fluorocholine uptake was not significantly increased with respect to background liver uptake in all 5 ICC cases (examples shown in **Figures 1** and **2**). The SUVmax of ICC tumors ranged from 4.1 to 7.6, while TBR ranged from 0.51 to 0.87. The SUVmax of ICC tumors was significantly lower than that of the 23 HCC tumors that had undergone gene expression profiling (mean SUVmax 5.5 vs. 12.2, p < 0.0001). TBR differed significantly between the
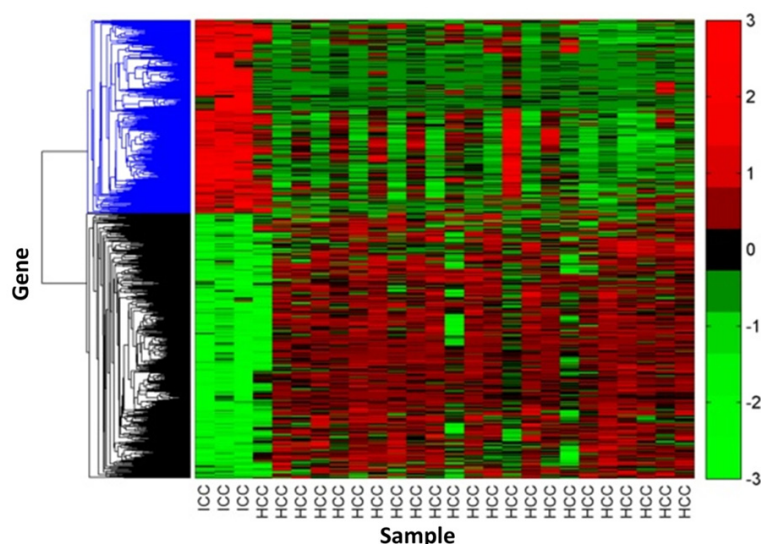
Figure 3. Row-clustered heat map of the 849-gene ICC signature. The first 3 columns represent ICC samples and the next 23 columns represent HCC samples. The color-coded entries represent the normalized expression of a given gene in a given sample. The heat map captures the heterogeneity that is inherent in the tumor samples while at the same time characterizing the transcriptional differences between the ICC and HCC tumors with high confidence (FDR = 2.5%). Note that the clustered heat map sharply discriminates the ICC samples from the HCC samples although some resemblance to ICC can be appreciated for the HCC sample that clustered closest to the ICC samples (sample 4).

ICC and HCC tumors (0.69 vs. 1.64, p < 0.0001), but there was no significant difference in mean liver SUV between the 5 ICC and 23 HCC patients (8.0 vs. 7.7, p = 0.74).

In two patients with ICC that also underwent clinical imaging with ^{18}F-FDG PET/CT, tumors demonstrated increased FDG uptake with a SUVmax of 10.6 in Patient 1 and a SUVmax of 9.6 in Patient 4. In Patient 1, the area of increased tumor FDG uptake correlated precisely with an area of diminished liver uptake on ^{18}F-fluorocholine PET (**Figure 1**). In Patient 4, the area of increased tumor FDG uptake corresponded on ^{18}F-fluorocholine PET/CT to iso-intense uptake along the tumor periphery and diminished uptake in the central part of the tumor (**Figure 2**). Small zones of focal necrosis were identified in the tumor specimen of Patient 4, although the extent of necrosis did not correspond to the spatial extent of diminished ^{18}F-fluorocholine uptake on PET/CT.

Expression array analysis

Differential expression analysis of the transcriptional array data resulted in a 849-gene signature that discriminated between the ICC

and HCC tumor samples with an empirical FDR of 2.5%. This is illustrated by a heat map in **Figure 3** where columns 1 to 3 represent 3 ICC samples and columns 4 to 26 represent 23 HCC samples. IPA analysis of the ICC signature revealed Farnesoid-X-receptor (FXR) activation as the most significant IPA canonical pathway (P = 1.7-e-43, 55/127 genes), with 53 of 55 ICC signature genes being down-regulated. Inhibition of lipid metabolism was a highly significant downstream effect predicted by the signature, involving numerous lipid related functions as summarized in **Table 3**. IPA analysis also identified a set of 12 significant upstream regulators of the 849-gene signature that included notable cancer-related genes such as TNF, IL1B, TGFB1, and Her2/Neu (**Table 4**). Individual signatures defined by each of these regulators, consisting of genes that were either directly or indirectly targeted by the regulator, were also submitted for pathway analysis, revealing the following states for all 12 regulators: 1) significant inhibition of FXR signaling and lipid metabolism, and 2) a predicted increase in glucose consumption due to over-expression of GLUT-1 and GLUT-3 via HIF1A signaling (**Table 4**).

Immunohistochemical analysis of protein expression

IHC analysis of glucose transporter and hexokinase expression was performed as a surrogate indicator of tumor glycolytic status to validate the findings from gene expression analysis. Tumors from all 5 patients with ICC demonstrated increased GLUT-1 expression relative to peritumoral liver tissue. However, GLUT-1 localization was predominantly cytoplasmic in the case of well-differentiated ICC while it more specifically localized to the cell membrane in the moderately-differentiated tumors. IHC expression of HK2 was also more intense or diffuse in the 4 moderately-differentiated tumors but decreased in the well-differentiated tumor. With regards to choline metabolism,

Table 3. The most significant downstream effects of the ICC signature on lipid metabolism

Lipid Function	P-Value	Activation Score	# Genes
Metabolism of terpenoid	6.57E-35	-2.720	76
Fatty acid metabolism	8.63E-34	-3.342	107
Oxidation of lipid	1.16E-21	-2.747	49
Transport of lipid	1.50E-17	-3.680	40
Metabolism of retinoid	1.85E-16	-2.401	22
Hydroxylation of lipid	5.10E-16	-2.744	16
Flux of lipid	5.57E-16	-3.935	31
Conjugation of lipid	9.42E-16	-3.065	13
Metabolism of tretinoin	8.69E-15	-2.083	16
Excretion of lipid	5.26E-14	-2.559	16
Efflux of lipid	5.27E-14	-3.595	28
Oxidation of fatty acid	7.93E-14	-2.043	34
Transport of steroid	1.45E-13	-3.291	22
Glucuronidation of lipid	4.89E-13	-3.058	10
Efflux of cholesterol	5.13E-12	-3.227	24
Efflux of phospholipid	4.42e-06	-1.988	8

Lipid functions are ordered by the intersection p-values of the genes associated with a given lipid function by IPA. Note that negative activation scores indicate inhibition of lipid function.

there was comparable expression of CKA between tumor cells and hepatocytes in 3 tumors and a heterogeneous but sparse pattern of marginally increased expression in one well-differentiated tumor and one moderately-differentiated tumor. Increased localization of HIF1α in the tumor cell nuclei was observed in all 4 moderately-differentiated tumors, while only increased cytoplasmic localization was noted in the well-differentiated tumor. Representative IHC images from Patient 5 are shown in **Figure 4**. Individual IHC results are summarized in **Table 1**.

Discussion

Many types of cancer harbor evidence of increased choline metabolism, including cancers of the breast, colon, prostate, lung, brain, and liver [11-15]. In a single-institution clinical trial, PET imaging using ^{18}F-fluorocholine, a positron-emitting synthetic substrate of CKA, was associated with a higher detection rate for HCC than conventional PET with FDG [6]. The results of the present pilot study, while derived from a limited number of patients, strongly suggest that ICC may be elusive to detection on the basis of ^{18}F-fluorocholine uptake, and despite being another primary liver malignancy, may

differ substantially from HCC with regards to the consumption of metabolic substrates. While it is disappointing that ^{18}F-fluorocholine PET/CT alone may not be useful for primary detection of ICC, the metabolic differences between ICC and HCC, as preliminarily identified in this study, may be helpful in further developing molecular imaging strategies for differentiating liver tumors.

We are not aware of any previous study of ICC using ^{18}F-fluorocholine PET/CT. Currently, ^{18}F-fluorocholine is not clinically available in many countries. The ICC tumors in this study consistently exhibited poor avidity for ^{18}F-fluorocholine in the absence of significant tumor necrosis that could have otherwise explained low accumulation of the tracer. Furthermore, differential expression analysis between ICC and HCC tumors linked ICC with the activation of regulatory molecules that may inhibit lipid pathways through direct and indirect effects on their downstream targets. Notably, 12 significant upstream regulators of a gene signature that differentiated ICC from HCC were predicted to inhibit farnesoid X-receptor (FXR) activation. FXR is a nuclear receptor known to be involved in the regulation of hepatic glucose, lipid, and bile acid metabolism that has also recently been implicated in the development of HCC [16, 17].

While differential expression analysis involving tumors is usually conducted as a comparison between malignant and corresponding normal tissue, the approach taken in the present study was to compare gene expression between ICC and HCC. We reasoned that since HCC tumors typically demonstrate increased ^{18}F-fluorocholine uptake relative to liver tissue(6), the differential signature between ICC and HCC would be better for identifying genes associated with tumor metabolic PET phenotype. Differential expression analysis between ICC and HCC may also serve to "filter out" mutually-expressed cancer-related genes, and aid in identifying the most significant molecular pathways for distinguishing these two types of primary liver cancer.

Table 4. Top upstream regulators of the ICC signature and their downstream effects

| Upstream Regulator	IPA Score	Intersection P-Value	Number of Genes in Signature	P-Value for GLUT1/3 Activation via HIF1A	P-Value for Inhibition of FXR Activation & Lipid Metabolism
TNF	3.829	4.82e-29	345	6.64e-07	2.11e-35
IL1B	4.513	1.66e-21	293	1.83e-06	1.60e-38
TGFB1	5.545	8.68e-21	345	6.64e-07	5.42e-34
IL6	2.683	2.55e-20	360	1.06e-05	4.34e-44
IL1	2.347	1.24e-16	267	5.00e-07	5.00e-35
Her2/neu	2.917	8.67e-16	270	5.49e-07	4.41e-21
NR0B2	3.175	2.26e-14	393	9.92e-05	4.21e-49
EGFR	3.888	9.45e-13	288	8.42e-06	4.35e-31
HIF1A	3.141	4.04e-11	273	1.42e-06	2.00e-25
ERK1/2	3.195	1.52e-07	286	9.42e-07	2.48e-24
P38/MAPK	3.063	7.59e-07	302	1.24e-05	4.03e-36
VEGF	2.710	1.79e-06	228	1.22e-06	1.67e-21

A signature for a given regulator is composed of its direct and indirect downstream targets in the ICC signature. The upstream regulators are ordered by intersection P-Value. For each regulator shown, IPA score, intersection P-Value, signature size, and p-values for GLUT1/3 activation in ICC via HIF1A signaling and inhibition of FXR Activation and lipid metabolism are given. Scores greater than 2.0 and intersection P-values less than 1.0e-05 are considered significant.

While our results are limited by the number of patients being studied, transcriptomic and IHC analyses were in agreement in suggesting glucose metabolism to be more promising than choline metabolism as the basis for detecting ICC. Therefore, these molecular profiling results corroborate with the negative findings of this pilot imaging study. While ¹⁸F-fluorocholine PET/CT may have limited utility for the primary detection of ICC, clinical PET studies have previously shown FDG PET/CT to have a reasonably high detection rate for ICC in the range of 70 to 90% [18, 19]. This is in contrast to HCC, for which FDG PET has been shown to have low sensitivity for detecting the primary tumor (6, 20). A potential molecular basis for ICC detection with FDG PET may be an increase in tumor GLUT1 and HK2 expression, and indeed, the expression of these proteins has been correlated with increased tumor FDG uptake on PET imaging in moderately- and poorly-differentiated cholangiocarcinoma [21, 22]. In contrast, GLUT1 expression has not been found to correlate strongly with tumor FDG uptake in HCC [23]. Notably, well-differentiated ICC may exhibit a weaker glycolytic phenotype [21]. This pattern was also noticed in the present study with the lower expression of glycolysis-related markers by a well-differentiated tumor.

Discordant tumor avidity for ¹⁸F-fluorocholine and FDG may signify coincident changes in the pathways regulating phospholipid and glucose metabolism in ICC. In the present study, the molecular basis of these dual metabolic alterations was investigated by gene expression profiling and IHC analysis. While less is known about choline metabolism in ICC, hyperglycolysis and overexpression of GLUT-1 has been associated with tumor biologic aggressiveness and poor clinical outcome in ICC [21]. In the present study, increases in glucose transporter expression in ICC were associated with HIF1A signaling, and, multiple cancer-related genes were identified by pathway analysis as potentially driving this process. Conversely, the suppression of lipid metabolism pathways and FXR signaling, as predicted by this same gene signature, also helped to explain the low tumor avidity for ¹⁸F-fluorocholine seen in ICC.

This single-institution clinical pilot study of ICC has inherent limitations typical of small cohort studies. Furthermore, patients were recruited through a single referral center, and not all patients received a correlative clinical FDG PET scan or contributed sufficient tissue for gene expression analysis. Each of these factors raise the potential for bias. Furthermore, IHC validation of protein expression and metabolic PET phenotype was performed using a limited selection of research antibodies that may not be sufficient in characterizing the overall state of cellular metabolic proteins. For example, while ¹⁸F-fluorocholine is a synthetic substrate of CKA, tumor CKA expression may not neces-
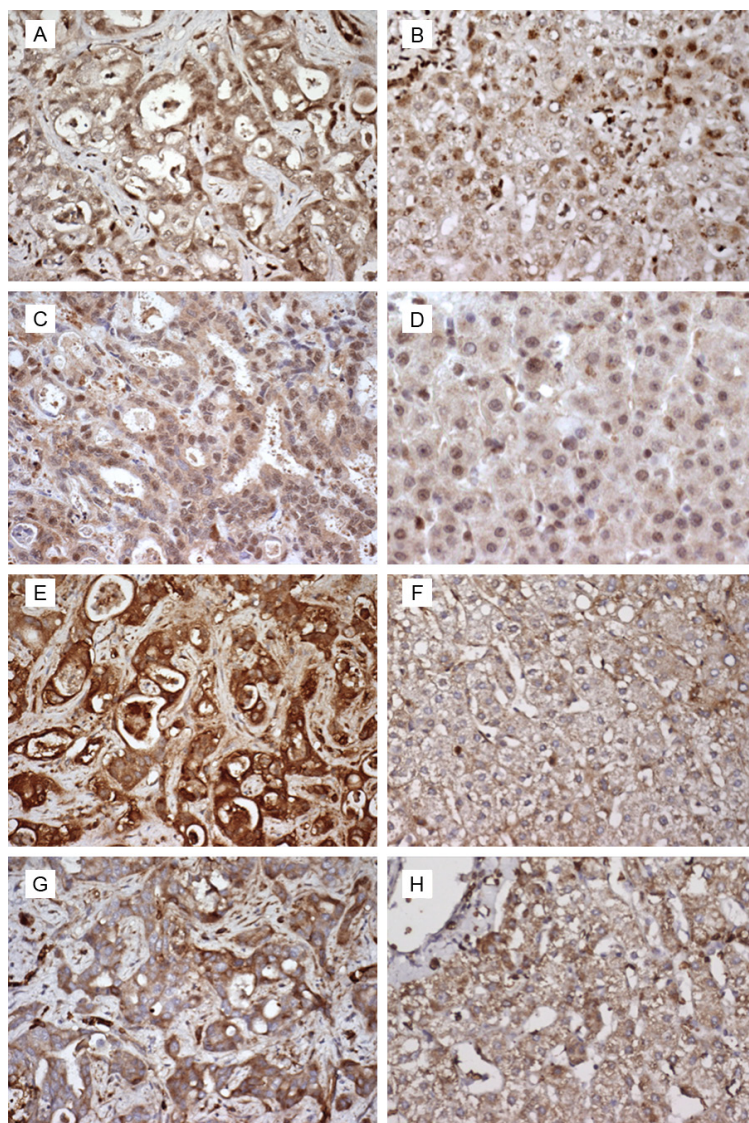
Figure 4. Histology images from Patient 1 at 400X shows immunohistochemical expression of choline kinase alpha (CKA) (A and B), HIF1α (C and D), hexokinase (E and F), and glucose transporter-1 (GLUT-1) (G and H) in tumor and adjacent parenchymal liver tissue, respectively (tumor A, C, E, G; liver B, D, F, H). Protein expression of CKA in tumor cells was comparable to native hepatocytes, while HIF1α, hexokinase, and membrane GLUT-1 protein expression was increased in tumor cells.

strongly with tissue choline transporter expression [25]. Thus, additional work may be required to fully explain in terms of protein expression the observed PET phenotypes.

Despite these limitations, the present study identified several coherent relationships between in-vivo imaging, histopathology, and genomics that allude to metabolic disturbances that may differentiate between ICC and HCC. More research involving a greater number of patients and samples will be needed to confirm the molecular mechanisms underlying these metabolic alterations in ICC and HCC, their relationship to metabolic PET imaging, and their prognostic and therapeutic relevance to patients with liver cancer.

Conclusion

Liver cancer is one of two cancers in the United States that is increasing in frequency [1]. The rising incidence of both ICC and HCC with increasingly similar risk factor profiles and clinical presentation, and yet disparity in clinical outcome, underscore the need for specific biomarkers for these two types of liver cancer. In addition to revealing metabolic and transcriptomic differences between ICC and HCC, the present study illustrates how molecular imaging may be able to detect differences between these two cancers that would otherwise not be identified in a conventional clinical workup.

sarily reflect tumor avidity for 18F-fluorocholine on PET imaging since intracellular accumulation of 18F-fluorocholine is dependent on *both* its membrane transport and intracellular phosphorylation [13]. This could explain why IHC analysis in this study did not reveal decreased protein expression of CKA in all ICC tumors as would otherwise be predicted by the low TBR on 18F-fluorocholine PET/CT. Tumor 18F-fluorocholine uptake may have correlated more

Acknowledgements

Disclosure of conflict of interest

None.

Authors' contribution

Study conception (LLW, GSO, SAK), design (LLW, GSO, OTMC, MT, SAK), implementation (LLW, GSO, OTMC, MT, SAK); data acquisition (LLW, GSO, OTMC, MT, SAK), analysis (LLW, GSO, OTMC, MT, SAK), and interpretation (LLW, GSO, OTMC, MT, SAK); drafting and revision of the article (LLW, GSO, OTMC, MT, SAK).

Abbreviations

FDG, ^{18}F-fluoro-D-deoxyglucose; HCC, hepatocellular carcinoma; ICC, intrahepatic cholangiocarcinoma; GLUT-1, glucose transporter 1; ECC, extrahepatic cholangiocaricnoma; CT, computed tomography; CA19-9, cancer antigen 19-9; PET, positron emission tomography; ROI, region of interest; SUV, standardized uptake value; TBR, tumor to mean background ratio; SUVmax, maximum SUV; FDR, false discovery rate; IPA, Ingenuity Pathway Analysis; IHC, immunohistochemical; CKA, choline kinase alpha; HK2, hexokinase 2 and HIF1A, hypoxia inducible factor 1 alpha.

Address correspondence to: Dr. Sandi A Kwee, The Queen's Medical Center, Honolulu, Hawaii, USA. Tel: 1-808-691-5466; E-mail: kwee@hawaii.edu

References

[1] Altekruse SF, Petrick JL, Rolin AI, Cuccinelli JE, Zou Z, Tatalovich Z and McGlynn KA. Geographic variation of intrahepatic cholangiocarcinoma, extrahepatic cholangiocarcinoma, and hepatocellular carcinoma in the United States. PLoS One 2015; 10: e0120574.

[2] Palmer WC and Patel T. Are common factors involved in the pathogenesis of primary liver cancers? A meta-analysis of risk factors for intrahepatic cholangiocarcinoma. J Hepatol 2012; 57: 69-76.

[3] Baheti AD, Tirumani SH, Rosenthal MH, Shinagare AB and Ramaiya NH. Diagnosis and management of intrahepatic cholangiocarci-noma: a comprehensive update for the radiologist. Clin Radiol 2014; 69: e463-70.

[4] Hu XX and Yan LN. Retrospective analysis of prognostic factors after liver transplantation for intrahepatic cholangiocarcinoma in China: a single-center experience. Hepatogastroenterology 2011; 58: 1255-9.

[5] Maithel SK, Gamblin TC, Kamel I, Corona-Villalobos CP, Thomas M and Pawlik TM. Multidisciplinary approaches to intrahepatic cholangiocarcinoma. Cancer 2013; 119: 3929-42.

[6] Talbot JN, Fartoux L, Balogova S, Nataf V, Kerrou K, Gutman F, Huchet V, Ancel D, Grange JD and Rosmorduc O. Detection of hepatocellular carcinoma with PET/CT: a prospective comparison of 18F-fluorocholine and 18F-FDG in patients with cirrhosis or chronic liver disease. J Nucl Med 2010; 51: 1699-706.

[7] Lim J, Dorman E and Cabral C. Automated Production of [18F]FECh and [18F]FCH: Preparation and Use of [18F]Fluoroalkane Sulfonates and Fluoroalkylation Agents [abstract]. J Label Compd Radiopharm 2003; 46: S46.

[8] Lin SM, Du P, Huber W and Kibbe WA. Model-based variance-stabilizing transformation for Illumina microarray data. Nucleic Acids Res 2008; 36: e11.

[9] Kwee SA, Chan O, Kawahara J, Hernandez B and Wong L. Tissue microarray expression of PET imaging biomarkers in hepatocellular caricnoma. J Nucl Med 2012; 53 Suppl 1: 1106.

[10] van Diest PJ, van Dam P, Henzen-Logmans SC, Berns E, van der Burg ME, Green J and Vergote I. A scoring system for immunohistochemical staining: consensus report of the task force for basic research of the EORTC-GCCG. European Organization for Research and Treatment of Cancer-Gynaecological Cancer Cooperative Group. J Clin Pathol 1997; 50: 801-4.

[11] Ramirez de Molina A, Rodriguez-Gonzalez A, Gutierrez R, Martinez-Pineiro L, Sanchez J, Bonilla F, Rosell R and Lacal J. Overexpression of choline kinase is a frequent feature in human tumor-derived cell lines and in lung, prostate, and colorectal human cancers. Biochem Biophys Res Commun 2002; 296: 580-3.

[12] Kwee SA, Hernandez B, Chan O and Wong L. Choline kinase alpha and hexokinase-2 protein expression in hepatocellular carcinoma: association with survival. PLoS One 2012; 7: e46591.

[13] Bansal A, Shuyan W, Hara T, Harris RA and Degrado TR. Biodisposition and metabolism of [(18)F]fluorocholine in 9L glioma cells and 9L glioma-bearing fisher rats. Eur J Nucl Med Mol Imaging 2008; 35: 1192-203.

[14] Glunde K, Jie C and Bhujwalla ZM. Molecular causes of the aberrant choline phospholipid

metabolism in breast cancer. Cancer Res 2004; 64: 4270-6.

[15] Kuang Y, Salem N, Tian H, Kolthammer JA, Corn DJ, Wu C, Wang F, Wang Y and Lee Z. Imaging lipid synthesis in hepatocellular carcinoma with [methyl-11c]choline: correlation with in vivo metabolic studies. J Nucl Med 2011; 52: 98-106.

[16] Huang XF, Zhao WY and Huang WD. FXR and liver carcinogenesis. Acta Pharmacol Sin 2015; 36: 37-43.

[17] Gadaleta RM, Cariello M, Sabba C and Moschetta A. Tissue-specific actions of FXR in metabolism and cancer. Biochim Biophys Acta 2015; 1851: 30-9.

[18] Petrowsky H, Wildbrett P, Husarik DB, Hany TF, Tam S, Jochum W and Clavien PA. Impact of integrated positron emission tomography and computed tomography on staging and management of gallbladder cancer and cholangiocarcinoma. J Hepatol 2006; 45: 43-50.

[19] Corvera CU, Blumgart LH, Akhurst T, DeMatteo RP, D'Angelica M, Fong Y and Jarnagin WR. 18F-fluorodeoxyglucose positron emission tomography influences management decisions in patients with biliary cancer. J Am Coll Surg 2008; 206: 57-65.

[20] Khan MA, Combs CS, Brunt EM, Lowe VJ, Wolverson MK, Solomon H, Collins BT and Di Bisceglie AM. Positron emission tomography scanning in the evaluation of hepatocellular carcinoma. J Hepatol 2000; 32: 792-7.

[21] Kubo Y, Aishima S, Tanaka Y, Shindo K, Mizuuchi Y, Abe K, Shirabe K, Maehara Y, Honda H and Oda Y. Different expression of glucose transporters in the progression of intrahepatic cholangiocarcinoma. Hum Pathol 2014; 45: 1610-7.

[22] Paudyal B, Oriuchi N, Paudyal P, Higuchi T, Nakajima T and Endo K. Expression of glucose transporters and hexokinase II in cholangiocellular carcinoma compared using [18F]-2-fluro-2-deoxy-D-glucose positron emission tomography. Cancer Sci 2008; 99: 260-6.

[23] Lee JD, Yang WI, Park YN, Kim KS, Choi JS, Yun M, Ko D, Kim TS, Cho AE, Kim HM, Han KH, Im SS, Ahn YH, Choi CW, Park JH. Different glucose uptake and glycolytic mechanisms between hepatocellular carcinoma and intrahepatic mass-forming cholangiocarcinoma with increased (18)F-FDG uptake. J Nucl Med 2005; 46: 1753-9.

[24] AAndersen JB, Spee B, Blechacz BR, Avital I, Komuta M, Barbour A, Conner EA, Gillen MC, Roskams T, Roberts LR, Factor VM, Thorgeirsson SS. Genomic and genetic characterization of cholangiocarcinoma identifies therapeutic targets for tyrosine kinase inhibitors. Gastroenterology 2012; 142: 1021-1031, e15.

[25] Inazu M. Choline transporter-like proteins CTLs/SLC44 family as a novel molecular target for cancer therapy. Biopharm Drug Dispos 2014; 35: 431-49.